

Ultrafast Imaging and the “Phase Problem” for Inelastic X-Ray Scattering

By *Peter Abbamonte, Gerard C. L. Wong, David Cahill, James P. Reed, Robert H. Coridan, Nathan W. Schmidt, Gee Hwee Lai, Yu Gan, Young Il Joe**, *Diego Casa, Tim Graber*[†]

[*] P. Abbamonte, D. Cahill, G. C. L. Wong, J. P. Reed, R. Coridan, Yu Gan, Young Il Joe
Frederick Seitz Materials Research Laboratory
University of Illinois
Urbana, IL, 61801 (USA)
E-mail: abbamonte@mrl.uiuc.edu

[[†]] D. Casa, T. Graber
Advanced Photon Source
Argonne National Laboratory
Argonne, IL, 60439 (USA)

This review gives an introduction to a new method for using inelastic x-ray scattering (IXS) to image ultrafast dynamics in condensed matter. We describe, in general terms, the concepts of causality and irreversibility in nature, and show how they are expressed in propagators for various physical observables. These concepts lead to a general solution of the inverse scattering problem (or “phase problem”) for inelastic x-ray scattering, which allows direct imaging of electron dynamics with resolutions close to 1 attosecond (10^{-18} sec) in time and less than 1 Å in space. This method is not just a Fourier transform of IXS data, but a means to impose causality on IXS data reconstruct the charge propagator. The method can also be applied to inelastic electron or neutron scattering. We give a general picture of phenomena that can and cannot be studied with this technique, and provide an outlook for the future.

1. Dynamics, Irreversibility, and Causality

Dynamics is the study of the way physical phenomena evolve in time. A central goal in the study of dynamics is to determine cause and effect relationships between phenomena, from which one can test models and make predictions.

As a rudimentary example, consider a ceramic dish dropped above a stone floor. When the dish strikes the floor it will certainly shatter. In this situation we can say that the shattering of the dish was “caused” by the dropping. That is, the dropping and the shattering have a causal relationship, the latter following from the former, and not the reverse.

The concept of causality is intuitive. However, causality is meaningful only for a large ensemble of particles, such as the pieces that make up the dish. For a few-body system, the concept of causality is ill-defined. To understand why, consider another rudimentary example, of two children playing catch with a baseball. Alice throws the ball, which follows a parabolic trajectory in accordance with Newton’s laws, and caught by Bob. We then ask if there is an intrinsic causal relationship between the ball’s departure (A) and its arrival (B) events, analogous to the dish example. To gain some insight we record a video of the game, and play it backward in time. When we do, we see that the ball back-tracks along its trajectory, but still satisfies Newton’s laws. We conclude, then, that there is nothing intrinsically causal about the relationship between A and B; either can follow from the other. The reason is that Newton’s laws are “time-reversal invariant”, i.e. they are unchanged even if the flow of time is reversed. Time reversal invariance is very general in physics, and applies equally well to quantum phenomena. The many-body Schrödinger equation, for example, is also time-reversal invariant. [1]

So how can the shattering dish exhibit such clear causality? In a many-body system, processes that are time-reversal invariant in principle can become irreversible in practice, because of the difficulty in meeting the initial conditions of the time-reversed state. To see how, suppose we played the shattering dish in reverse. We would see a collection of

fragments reassemble into a dish, and then rise into the air. Clearly, such a process could never occur. The reason is not that the process violates Schrödinger's equation, which it certainly does not, but that the set of initial velocities of all the fragments is so unlikely to occur that the probability of ever seeing such an event is infinitely small. Unlike the thrown baseball, then, the breaking of a dish is *irreversible*, with a well-defined cause (the dropping) and effect (the shattering), i.e. well-defined causality.

More concisely, the concept of causality is not definable microscopically. As originally observed by Eddington [2], there is no microscopic "arrow of time" in nature. Our perception of cause and effect, and of time "flowing" in a particular direction, is not fundamental, but a result of the accumulation of randomness in collections of particles. This randomness is captured by the quantity "entropy", whose perpetual rise is dictated by the second law of thermodynamics. Nothing about causality is contained in the microscopic laws of physics, however, and the concepts of "past" and "future" are meaningful only in a statistical sense, the rise of entropy being the determiner of time's arrow.

Returning to the subject of dynamics, measuring cause and effect has become a major field of research. In recent years there has been an explosion of new technology for ultrafast pump-probe experiments, which have allowed studies of dynamics on ultrashort time scales. Pump-probe methods work by perturbing the system with a short laser pulse, and then probing it with a second, timed to arrive after a controlled delay. These techniques made a large impact in the study of the femtosecond transient states that occur during an irreversible (in the sense defined above) chemical reaction. [3] The advent of high harmonic generation techniques are now driving this field to the next level – the attosecond regime – to study electron dynamics. [4,5]

In this article we describe a different and complementary approach to studies of ultrafast phenomena, based on inelastic x-ray scattering (IXS), using synchrotron x-ray sources. We will explain, how the concepts of causality and irreversibility may be used to

solve the so-called “inverse scattering problem” for IXS, providing a general strategy for imaging dynamics in many-electron systems. One of the essential advances has been improvement in technology for synchrotron experiments, which provided the improvement in data quality needed for inversion algorithms to work. This technique can access both the femtosecond and attosecond time regimes, and also provides angstrom level spatial imaging.

This technique may seem completely different from the more familiar pump-probe approach. We will, however, point out a surprisingly precise connection between the two approaches, that suggests – through analogy – a deeper meaning of the term “dynamics”. We will describe the kinds of phenomena that can be studied with this technique, what phenomena cannot, and where it falls in the spectrum of methods for studying ultrafast dynamics.

2. The Propagator

The most general quantity describing the dynamics of a system is its “propagator”. To begin, suppose a system is described by the Schrödinger wave equation

$$\left\{ \hat{H}(t) + \frac{i}{\hbar} \frac{\partial}{\partial t} \right\} |\Psi\rangle = 0 \quad (1)$$

where H is a Hamiltonian and $|\Psi\rangle$ is a many-body state describing the system. The retarded propagator, G_R , is defined as

$$G_R = -\frac{i}{\hbar} \langle 0 | \left\{ \hat{H}(t) + \frac{i}{\hbar} \frac{\partial}{\partial t} + i\gamma \right\}^{-1} | 0 \rangle \theta(t) \quad (2)$$

where $|0\rangle$ is the ground state, the “-1” exponent indicates a matrix inverse, where γ is a small parameter that prevents the inverse from diverging. The propagator, physically, describes the probability that the system will evolve from one configuration at time $t = 0$ to another at time t .

Unlike the Hamiltonian, H , the propagator G_R contains information about causality. The analytic properties of G_R are chosen to impose a cause and effect relationship between the

excitations of the system, in effect phasing them properly in time. G_R is, as a result, an explicit measure of the dynamics of the system.

Various conventions for causality may be chosen. For the case of the retarded propagator, G_R , the dynamics take place only for $t > 0$, and entropy always increases. One could, alternatively, choose an advanced propagator, G_A , which is nonzero only for $t < 0$ and entropy always decreases (i.e. G_A is time time-reversed version of G_R). Time-ordered and other conventions may also be used [6]. The convention chosen is arbitrary – similar to the use of retarded versus advanced potentials in electrodynamics – and is a matter of choosing a sign convention for γ .

G_R describes everything that can be known about the dynamics of a system. Unfortunately, it is usually impossible to determine completely. A traditional approach, then, is to seek propagators not for the entire system, but specific physical observables, such as the electron density, local magnetic moment, etc., which can be related to G_R through physical models.

3. Inelastic X-Ray Scattering (IXS) and its Inverse Problem

Propagators can be determined from scattering experiments. The measured intensity in scattering is proportional to the imaginary part of the propagator for some physical observable [7]. Scattering experiments are, in principle, a direct way to probe the dynamical properties of many-particle systems [7]. IXS, for example, probes the dynamical properties of the total electron density. Inelastic electron scattering, often referred to as electron energy loss spectroscopy (EELS), probes the total charge density (including both electrons and nuclei). Inelastic neutron scattering detects the nuclei and the local magnetic moment.

An IXS experiment is done by directing a collimated, monochromatic beam of x-rays at a specimen, and measuring the intensity of x-rays scattered at different angles and energies. If the incident photon energy is kept far from all the core absorption levels, resonant processes

will be suppressed and the dominant scattering process will be the “seagull diagram” shown in Fig. 1.[8] The scattered intensity will then be proportional to the dynamic structure factor [7,9]

$$S(\mathbf{k}, \omega) = \sum_{m,n} |\langle m | \hat{n}(\mathbf{k}) | n \rangle|^2 P_n \delta(\omega - \omega_m + \omega_n) \quad (3)$$

Where $|n\rangle$ is an eigenstate of the electronic system, ω is the energy transferred to the sample by the photon, \mathbf{k} is the momentum transfer, and $P_n = \exp[-E_n/k_B T]$ is the Boltzmann factor. $\hat{n}(\mathbf{k})$ is an operator for the total electron density, and the delta function imposes energy conservation.

The dynamic structure factor is the Fourier transform of the Van Hove space-time correlation function for the electron density

$$C(\mathbf{x}, t) = \int dx' dt' \langle \hat{n}(\mathbf{x}, t) \hat{n}(\mathbf{x} + \mathbf{x}', t + t') \rangle \quad (4)$$

where $\langle \dots \rangle$ denotes a quantum mechanical, thermal average [9]. C describes the degree to which the electron density at the origin at time $t=0$ is correlated with that at position \mathbf{x} at some later time t . This correlation function, which can be obtained just by Fourier transforming the data, contains some information about dynamics, in the sense that its value is determined by the properties of excited states of the system. However, C has no causal properties, so its relation to dynamics is indirect.

Fortunately, S is also related to the propagator for the electron density by the quantum mechanical version of the Fluctuation-Dissipation theorem,

$$S(\mathbf{k}, \omega) = \frac{1}{\pi} \frac{1}{1 - e^{\hbar\omega/k_B T}} \text{Im}[\chi(\mathbf{k}, \omega)] \quad (5)$$

where the retarded propagator χ is defined as

$$\chi(x, t) = -\frac{i}{\hbar} \langle [\hat{n}(x, t), \hat{n}(0, 0)] \rangle \theta(t) \quad (6)$$

Here $n(\mathbf{x},t)$ is an operator for the total electron density, $[,]$ is a commutator, and $\theta(t)$ is a step function. Physically, χ describes the probability that a disturbance in the electron density at the origin at time $t=0$ will propagate to position \mathbf{x} at some later time t .

Unlike $C(\mathbf{x},t)$, $\chi(\mathbf{x},t)$ is a direct measure of electron dynamics. As a true propagator, χ is causal, it properly phases excitations in time, and it adheres to the second law of thermodynamics, i.e. it always exhibits rising entropy.

Unfortunately, reconstructing χ from S is not as simple as performing a Fourier transform. The experiment provides only the imaginary part, $Im[\chi]$. We therefore have only a subset of the total data needed. To view the dynamics explicitly, we must solve the so-called “inverse scattering problem” for IXS.

Inverse problems, sometimes colloquially referred to as “phase problems”, are innate to all scattering techniques. They are encountered in subjects as diverse as ultrasonic imaging [10], geophysical surveying [11], radar [12], structural biology [13], coastal evolution [14], and in pure mathematics in the study of coupled differential equations [15]. In all cases, the solution involves using preexisting knowledge of the specimen to set constraints that, if combined with the scattering data, yield the missing information. To study dynamics explicitly, we must find such a constraint for the density propagator, χ .

4. Causality as a Solution to the Inverse Scattering Problem for IXS

To find a solution to the inverse problem it helps to have a deeper understanding of what information was lost by the experiment. As discussed earlier, propagators (unlike Hamiltonians) exhibit causality. The convention for causality is arbitrary; one may work with a retarded, advanced, time-ordered, or other propagator. The space-time behavior of these propagators is different, e.g. $\chi_R(\mathbf{x},t)$ exhibits rising entropy, and $\chi_A(\mathbf{x},t)$ exhibits falling entropy. However, all these conventions have a common trait: If transformed into (\mathbf{k},ω) space,

all these propagators have the same imaginary part. In reciprocal space, the various causal conventions differ only in their real part.

In other words, the information that is lost in an IXS experiment, which provides only $\text{Im}[\chi(\mathbf{k},\omega)]$, is the causality itself. Causality is not definable microscopically, and an IXS experiment provides only microscopic information. To solve the inverse problem, we need a recipe for re-integrating causality with the data from the experiment.

In ref. 16 we presented such a recipe. It involves four steps. The first is to symmetrize the data, to extract the quantity $\text{Im}[\chi(\mathbf{k},\omega)]$. This can be done by dividing by the Bose factor in eq. (5), or more cleanly from

$$\text{Im}[\chi(\mathbf{k},\omega)] = -\pi[S(\mathbf{k},\omega) - S(\mathbf{k},-\omega)] \quad (7)$$

which does not require knowledge of the sample temperature. Second, one must analytically continue the data, for example with linear interpolation, which is necessary to preserve causality in the final result. Third, one performs a sine transform of the imaginary part, i.e.

$$\chi(\mathbf{k},t) = 2 \int d\omega \text{Im}[\chi(\mathbf{k},\omega)] \cdot \sin(\omega t) \quad (8)$$

The fourth and final step is a standard spatial Fourier transform from $\chi(\mathbf{k},t)$ to $\chi(\mathbf{x},t)$. This procedure imposes retarded causality onto the data, resulting in a retarded propagator, $\chi(\mathbf{x},t)$, which is nonzero only at $t > 0$ and exhibits increasing entropy.

It has been incorrectly stated that our procedure is a “Fourier transform of IXS data”. [17] This statement is patently false. Simple Fourier transformation would yield, as said before, the correlation function, $C(\mathbf{x},t)$, which has no causal properties. Our method is a practical and general solution to the phase problem for IXS, and a way to directly study dynamics of many-particle systems by explicitly determining the charge propagator.

5. Experiment

An IXS experiment must be carried out at a synchrotron. Apart from this constraint, the experiment is rather simple. A typical layout for a moderate energy resolution ($\Delta\omega \sim 50$ -100 meV) experiment is shown in Fig. 1. A synchrotron is an electron storage ring comprising of a lattice of dipole, quadrupole, hexapole and in some cases octapole magnets, separated by straight sections. In these sections reside insertion devices, which are the source of x-rays. The most commonly used insertion device is an undulator, which is a series of dipole magnets whose spacing and field strength are tuned to create constructive interference at specified wavelengths (typically 1 Å) [18]. Its output is a well-collimated, broadband beam of marginally coherent hard x-rays, with a bandwidth of ~ 50 eV.

To make this beam suitable for scattering experiments, it is passed through a monochromator comprising two, nondispersively mounted, Bragg reflecting crystals (Fig. 1). The first bounce makes the beam monochromatic and the second redirects it along the beam path. At third generation synchrotrons, where the power density is rather high, monochromatization is usually done in two steps, a premonochromator that is cooled to absorb the heat load, followed by a secondary monochromator that narrows the bandwidth. This monochromatic beam passes through a series of slits and beam monitors, and strikes the specimen of interest, which is mounted at the center of a goniometer.

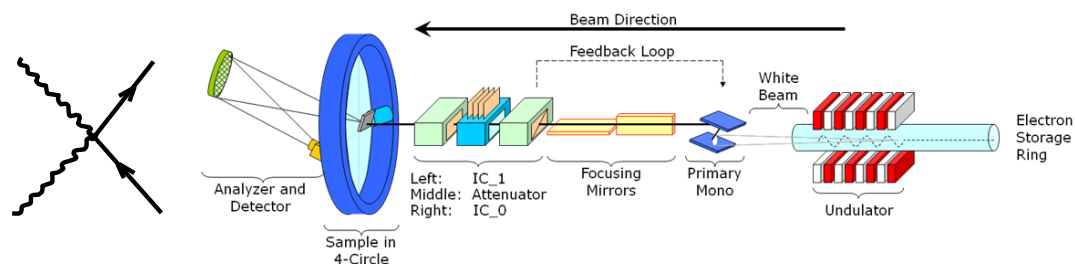


Figure 1 (left) Diagrammatic representation of the scattering process used in (nonresonant) inelastic x-ray scattering. This diagram is often referred to as the “seagull” diagram. (right) A typical, moderate energy resolution inelastic x-ray scattering setup, for measuring this scattering process.

The scattered x-rays must be energy-analyzed. This is accomplished with an “analyzer”, which is mounted on an arm that rotates around the sample position. The analyzer is a mosaic of $\sim 10^4$ tiny crystals (typically Si or Ge) mounted on a spherically curved substrate [17,19,20]. The analyzer works in backscattering geometry, reflecting the scattered x-rays onto a photon counting detector next to the sample. The energy transfer ω is then varied by rotating the angle of the monochromator, and the momentum transfer \mathbf{k} is varied by rotating the arm and sample goniometer angles. With such a setup one can routinely achieve momentum resolutions of less than 0.1 \AA^{-1} and energy resolution less than 100 meV, over a sufficiently broad range of energy and momentum to completely parameterize the cross section in eq. 5. Higher resolutions in energy can be obtained by using dispersively mounted, asymmetric reflections, or high order reflections in backscattering [20]. Higher momentum resolution can be obtained by masking the analyzer or lengthening the arm.

6. What Can be Learned from IXS Imaging?

What kind of phenomena can be studied with inverted IXS? An obvious strength is its unprecedented time resolution. As demonstrated in refs. [16,26], IXS imaging can routinely be done with resolutions better than 20 as. By pushing the technology, for example to higher energy, sub-attosecond i.e. zeptosecond time resolution should be achievable. The method therefore allows study of phenomena that are beyond the temporal reach of pump-probe technique. Another strength of the technique is its simultaneous access to spatial and temporal phenomena, at molecular length and time scales.

Not all phenomena are equally visible with IXS. Recall that its end result is the density propagator, $\chi(\mathbf{x}, t) = -i \langle [\hat{n}(\mathbf{x}, t), \hat{n}(0, 0)] \rangle \theta(t) / \hbar$. χ therefore reveals excitations that modulate the electron density [16]. IXS is therefore biased toward longitudinal, collective

modes, for example plasmons and longitudinal phonons. This bias is typified by our original study with this technique, which was to image the valence plasmon in liquid water [16].

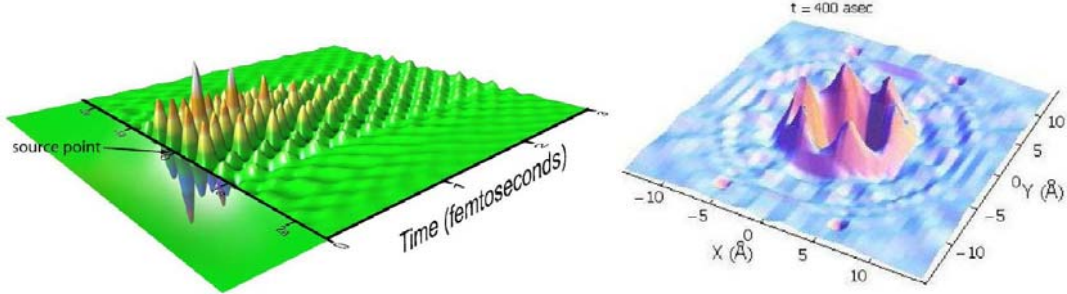


Figure 2 Examples of charge propagators, $\chi(\mathbf{x},t)$, reconstructed with our solution to the IXS inverse scattering problem. The propagator, physically, corresponds to the disturbance arising from a point source, and the location of this source is visible in these images. (left) $\chi(\mathbf{x},t)$ for LiF, showing time-evolution of the internal structure of the exciton. (right) $\chi(\mathbf{x},t)$ for a single crystal of graphite at time $t=400$ as. Visible are plasmons that contribute to the background dielectric constant.

A more recent application, done at Sectors 9 and 15 at the Advanced Photon Source (APS) was our imaging of the internal structure of the exciton in LiF. An exciton is a two-body bound state between a conduction electron and valence hole in an insulator, rather like positronium [21]. The first materials in which excitons were observed were the alkali halides, of which LiF is an example [21,26]. The excitons in these systems is of the “charge transfer” type, meaning they involve physical motion of charge from the alkali to the halide atom. This excitation therefore modulates the density and can be observed with IXS. For many years, it was debated whether the Frenkel or Wannier description was better suited to these systems [21]. By examining the time-evolution of its internal structure (Fig. 2), we were able to demonstrate that the exciton in LiF is best described by a Frenkel model [26].

Currently we are using inverted IXS to image collective excitations in graphite, using facilities at APS Sector 9 (Fig. 2). Graphite is a refractory material with unique physical properties and vast commercial uses. It is a quasi-two-dimensional material with an unusual Fermi surface consisting of small, nested pockets [22]. As a semimetal, graphite has a very

low carrier density, but nonetheless fails to exhibit strong correlation effects, i.e. is quite efficient at screening Coulomb interactions. To understand why, we have been using our images of collective excitations (Fig. 2) to observe the origin of local screening, which will explain the surprising ability of graphite to screen charge [23,24,25].

7. Analogy with Pump-Probe Techniques

Inverted IXS may seem, on the surface, completely unrelated to the more established pump-probe approach to studying ultrafast dynamics. The similarities, however, are deeper than they may seem.

To begin, one might think of the propagator itself as a simplistic pump-probe “experiment”. $\chi(\mathbf{x},t)$ is, by definition, the density disturbance generated by a point source. The source might be thought of as a “pump”, the ensuing dynamics being in a sense “probed” by the propagator.

What is the time resolution in this pseudo-pump-probe experiment? The resolution can be defined in terms of the Nyquist theorem, which gives a time resolution $\Delta t_N = \pi/\Omega_{max}$, where Ω_{max} is the range of transferred energies measured in the experiment [26]. In ref. 26 we referred to this quantity as a “Nyquist resolution”. The scan range Ω_{max} therefore, in a manner of speaking, plays the role of the pulse width.

Continuing the analogy, the energy resolution of the IXS experiment, $\Delta\omega$, plays the role of a repetition rate. To see why, note that the frequency integral eq. (8), at large t , must be done with steps that are much finer than $\Delta\omega$. This necessitates an analytic continuation to preserve causality and prevent leakage of density into negative times [16,26,27].

Continuation should be done with linear interpolation, which creates slope discontinuities in the spectra. These discontinuities, when transformed into time, cause the dynamics to repeat with a period $T = 2\pi/\Delta\omega$, rather like a pump-probe experiment. This repetition sets limits on

the duration over which excitations can be examined; phenomena that take place on a time scale longer than T cannot be observed. Slower phenomena can be studied by narrowing the bandwidth $\Delta\omega$, but this lowers the signal and decreases the statistical quality of the data, similar to lowering the repetition rate in a pump-probe experiment.

The broader point is that, ultimately, there is only one way to study dynamics, which is to perturb a system and examine how it returns to equilibrium. All experimental probes of dynamics, as different as they may seem on the surface, can be mapped onto this basic approach.

8. Sources and Superposition

The propagator $\chi(\mathbf{x},t)$ represents, physically, the response due to a delta function source at the origin. Because any function can be expressed as a superposition of delta functions, $\chi(\mathbf{x},t)$ permits one to reconstruct – within the assumption of linear response – the disturbance arising from an extended source. The density $n_{ind}(\mathbf{x},t)$ induced by a general time-dependent external charge density $n_{ext}(\mathbf{x},t)$ is given in reciprocal space by

$$n_{ind}(\mathbf{k}, \omega) = \frac{4\pi e^2}{k^2} \chi(\mathbf{k}, \omega) n_{ext}(\mathbf{k}, \omega) \quad (9)$$

This expression provides a simple way to model extended, time-dependent sources, properly accounting for coherent interference among excitations.

As an example, we recently used eq. 9, together with ultra-high resolution IXS data, to study hydration-like processes in liquid water. A molecular understanding of water is central to a broad range of physical phenomena. The short-range structure and dynamics of water has been the subject of intensive study with x-ray absorption spectroscopy [28,29], scattering techniques [30], ultrafast spectroscopy [31,32], such as IR “pump-probe” and vibrational-echo correlation spectroscopy experiments [33,34,35], and molecular dynamics

simulations [36]. Much of what we know about hydration comes from this body of experimental and theoretical/computational work on solvation dynamics [37].

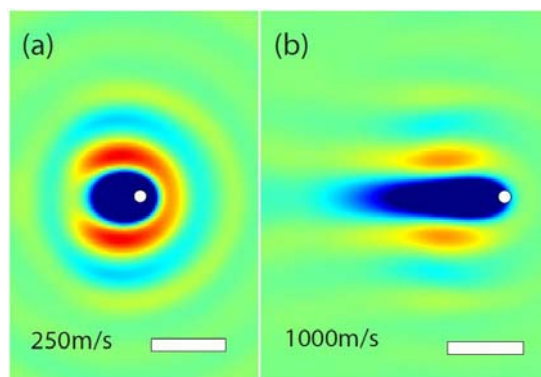


Figure 3 The hydration structure around a negative charge moving with a steady state linear velocity (a) $v=250\text{m/s}$, (b) $v=1000\text{m/s}$. Regions of oxygen-density enhancement (indicated by higher electron densities) are red and region of oxygen depletion are blue. The scale bar represents 3\AA .

By using a high resolution data set measured at several 3rd generation synchrotron facilities, including 3-ID at the Advanced Photon Source and ID-28 at the ESRF, we were able to reconstruct the charge propagator for liquid water at 26 femtosecond time resolution and 0.44\AA spatial resolution [27]. This time scale is long enough to observe the structural dynamics of water. IXS has been employed at these facilities to measure spectra reflecting collective dynamics in water [38,39], and the hydration and ionic environments surrounding different biopolymers [40,41]. Using the procedure outlined above, we took these studies a step further and reconstructed the full propagator. The water dynamics we observed is consistent with classical molecular dynamics (MD) simulations of diffusional relaxation, and to femtosecond spectroscopic measurements of the O-O dynamics.

To gain insight into hydration, we used this propagator, combined with eq. 9, to produce Fig. 3. This figure shows an abstract situation, the ‘steady state’ dynamical hydration structure around an idealized point negative charge. In the cross-section views (Fig. 3), regions of oxygen-density enhancement around a moving negative point charge are red and

region of oxygen depletion are blue. Even for velocities significantly less than the speed of sound in water v_s ($\approx 1600\text{m/s}$, a typical thermal velocity), the hydration structure deviates from the idealized spherically symmetric “hydration shell” usually assumed, and forms instead a hydration “bowl”, with a depletion of oxygen density in front of and especially behind the moving charge distribution. As the velocity increases to 1000 m/s , which is of the same order as v_s , the “hydration wake” is formed, and the hydration “bowl” transforms into a hydration “sleeve” (Fig. 3). These results suggest that a stationary molecule and a moving molecule may participate in chemical reactions differently in water.

9. What IXS Imaging Cannot Do

The time resolution of IXS can in principle be extremely high. However, not all excitations are visible with IXS. Like any other x-ray technique, it is only sensitive to phenomena with significant density contrast (see Section 6). Phenomena like spin waves, Wannier excitons, interband transitions in semiconductors, etc., are difficult or impossible to study with IXS.

Further, with existing technology, IXS is still limited to the regime of linear response. This makes IXS, for the moment, a passive imaging method. High field physics, second harmonic generation, three- and four- wave mixing, parametric up- or down-conversion, etc., are at the moment, for x-ray techniques, still relegated to the imagination.

The restriction of linear response can be cumbersome when working with extended sources. Returning to the hydration example (see Section 8), linear response dictates that the solvent relaxes through the same modes that govern fluctuations of the interaction at equilibrium. Linear response is believed to hold for most solute-solvent systems, in particular at length scales smaller than those that nucleate a change in phase in the surrounding solvent [42,43,44]. However, it has recently been demonstrated that linear response can fail for cases involving chemical reactions and photoexcitation [45], in which the excitation changes the

solute size, affecting the steric state as well as the energetics of hydration, rather than just the latter. Linear response can also break down for phenomena that are so rapid that they break the assumption of continuous solute-solvent interaction.

Some of these limitations can be overcome by using, instead of eq. 9, a fully self-consistent approach. For example, in the case of an asymmetric solute size, the initial and final charge distribution, as well as the initial and final size and shape of the excluded molecular volume may be included in the source itself, the solution being achieved by iteration to convergence. This strategy would mitigate against errors due to breakdown from changes in steric interactions due to changes in molecular shape. Experimentation with such approaches has only just begun.

The linear response limitation should not be overinterpreted. IXS is linear only in terms of the probe. When multiple excitations are simultaneously visible, for example a phonon and an exciton, the interaction between the two can be highly nonlinear.

Finally, IXS imaging – as currently implemented in our algorithms – provides only a spatially averaged response. In a system that lacks translational symmetry, the propagator is actually a function of two momenta, not just one, i.e. $\chi = \chi(\mathbf{k}_1, \mathbf{k}_2, \omega)$. Current IXS methods measure only the diagonal parts of this response, $\chi(\mathbf{k}, \omega) = \chi(\mathbf{k}, -\mathbf{k}, \omega)$. The resulting images are averages over all source locations [23]. For bulk materials, which have some translational symmetry, this is not a serious limitation. However finite systems with no translational symmetry, such as a single molecule, cannot be imaged. This limitation may be overcome with standing wave methods, however attempts to do so are in their earliest beginnings [16,23].

10. Outlook

The technique of IXS traces its origins to nuclear and high energy physics. The first x-ray facilities were beam lines running in a parasitic fashion on colliding beam facilities like

SPEAR and CESR. Conceptually, IXS is in the same class of experiment as, for example, the deep inelastic scattering measurements of the quark structure of the hadrons in the 1960s. Such accelerator approaches have, over the years, naturally evolved to lower energy to address length and time scales relevant to molecular, biological, and condensed matter systems. Today, most x-ray experiments are carried out at dedicated synchrotron light sources.

In parallel, pump-probe methods, once used for studying structural intermediates in chemical reactions, are being pushed to shorter time scales to address more fundamental issues of electron dynamics. To reach such time scales, experimenters are exploiting high harmonic generation techniques to go to higher energy where broader bandwidths are possible. It seems likely that these two communities will meet somewhere at an energy ~ 1 keV, and a revolution in ultrafast science will ensue.

Acknowledgements

We acknowledge Thomas Gog, Michael Krisch, and Alfred Baron for important scientific and technical input. This work was supported by the Office of Basic Energy Sciences, U.S. Department of Energy, DE-FG02-07ER46459, through the Frederick Seitz Materials Research Laboratory. Use of the Advanced Photon Source was supported by DOE Contract DE-AC02-O6CH11357. GW is supported by NSF Water CAMPWS and the RPI-UIUC NSEC (DMR-0117792, DMR-0642573).

-
- 1 There do exist examples in nature of fundamental time-reversal symmetry breaking. Weak nuclear forces, such as those involved in kaon decay, break time-reversal symmetry and lead to the matter-antimatter asymmetry in the universe. If time had been reversed, however, this would simply lead to reversal of the definitions of matter and antimatter.
 - 2 A. S. Eddington, *The Nature of the Physical World* (McMillan, Cambridge, 1948)
 - 3 A. Zewail, *J. Phys. Chem. A* **104**, 5660 (2000)
 - 4 P. H. Bucksbaum, *Science* **317**, 766 (2007)
 - 5 F. Krausz, M. Ivanov, *Rev. Mod. Phys.* **81**, 163 (2009)

-
- 6 It sometimes useful, for example if one needs to retain Lorentz invariance, to work with a time-ordered propagator, G_{TO} , which is the sum of G_R and G_A .
 - 7 Léon Van Hove, Phys. Rev. **95**, 249 (1954)
 - 8 Implicit here is the first Born approximation. Including this single diagram is equivalent to taking just the first Born amplitude. Linear response is a good approximation in the x-ray case because the cross section is weak.
 - 9 S. K. Sinha, J. Phys.: Cond. Mat. **13**, 7511 (2001)
 - 10 C. Sumi, A. Suzuki, K. Nakayama, IEEE Trans. Biomed. Eng. **42**, 193–202 (1995)
 - 11 R. L. Parker, Geophysical Inverse Theory (Princeton University Press, Princeton, 1994)
 - 12 B. Borden, Inverse Problems **18**, R1-R28 (2002)
 - 13 G. Taylor, Acta Crystallographica D **59**, 1881 (2003)
 - 14 M. Spivack, D. E. Reeve, J. Comput. Phys. **161**, 169 (2000)
 - 15 M. Ablowitz, P. Clarkson, Solitons, Nonlinear Evolution Equations and Inverse Scattering (Cambridge, 1991)
 - 16 P. Abbamonte, K. D. Finkelstein, M. D. Collins, S. M. Gruner, Imaging density, Phys. Rev. Lett., **92**, 237401 (2004)
 - 17 W. Schülke, Electron dynamics by inelastic x-ray scattering (Oxford, 2007)
 - 18 Such experiments are also commonly done in the soft x-ray (0.5-1 keV) range. However the “seagull” process in Fig. 1 is nearly impossible to measure in this case because of the small scattering volume.
 - 19 R. Verbeni, F. Sette, M. H. Krisch, U. Bergmann, B. Gorges, C. Halcoussis, K. Martel, C. Masciovecchio, J. F. Ribois, G. Ruocco, H. Sinn, J. Synchrotron Radiation **3**, 62 (1996)
 - 20 Yuri Shvydko, X-Ray Optics: High-energy resolution applications (Springer-Verlag, 2004)
 - 21 R. S. Knox, Theory of Excitons (Academic, New York, 1963).
 - 22 A. Bostwick, T. Ohta, T. Seyller, K. Horn, E. Rotenberg, Nature Physics **3**, 36 (2006)
 - 23 P. Abbamonte, J. P. Reed, Y. I. Joe, Yu Gan, D. Casa, arXiv:0904.0795
 - 24 J. P. Reed, et. al., preprint
 - 25 B. Uchoa et. al., preprint
 - 26 P. Abbamonte, T. Graber, J. P. Reed, S. Smadici, C.-L. Yeh, A. Shukla, J.-P. Rueff, Wei Ku, Proc. Natl. Acad. Sci. **105**, 12159 (2008)
 - 27 R. Coridan, et. al., preprint
 - 28 Wernet P, et al. (2004) The Structure of the First Coordination Shell in Liquid Water. *Science* 304(5673):995-999.
 - 29 Smith JD, et al. (2004) Energetics of Hydrogen Bond Network Rearrangements in Liquid Water. *Science* 306(5697):851-853.
 - 30 Head-Gordon T & Hura G (2002) Water Structure from Scattering Experiments and Simulation. *Chemical Review* 102(8):2651-2670.
 - 31 Franks F (1972) *Water: A Comprehensive Treatise* (Plenum Press, New York).
 - 32 Eisenberg D & Kauzmann W (1969) *The Structure and Properties of Water* (Oxford University Press, New York); trans Kauzmann W p 296.
 - 33 Woutersen S, Emmerichs U, & Bakker HJ (1997) Femtosecond Mid-IR Pump-Probe Spectroscopy of Liquid Water: Evidence for a Two-Component Structure. *Science* 278(5338):658-660.
 - 34 Woutersen S & Bakker HJ (1999) Resonant intermolecular transfer of vibrational energy in liquid water. *Nature* 402(6761):507-509.
 - 35 Fecko CJ, Eaves JD, Loparo JJ, Tokmakoff A, & Geissler PL (2003) Ultrafast Hydrogen-Bond Dynamics in the Infrared Spectroscopy of Water. *Science* 301(5640):1698-1702.
 - 36 Head-Gordon T & Johnson ME (2006) Tetrahedral structure or chains for liquid water. *Proceedings of the National Academy of Science* 103(21):7973-7977.

-
- 37 Maroncelli M, Macinnis J, & Fleming GR (1989) Polar Solvent Dynamics and Electron-Transfer Reactions. *Science* 243(4899):1674-1681.
 - 38 Sette F, *et al.* (1995) Collective Dynamics in Water by High Energy Resolution Inelastic X-Ray Scattering. *Physical Review Letters* 75(5):850.
 - 39 Sette F, *et al.* (1996) Transition from Normal to Fast Sound in Liquid Water. *Physical Review Letters* 77(1):83.
 - 40 Chen SH, *et al.* (2001) Collective Dynamics in Fully Hydrated Phospholipid Bilayers Studied by Inelastic X-Ray Scattering. *Physical Review Letters* 86(4):740.
 - 41 Angelini TE, *et al.* (2006) Counterions between charged polymers exhibit liquid-like organization and dynamics. *Proceedings of the National Academy of Science* 103(21):7962-7967.
 - 42 Pratt L R and Chandler D (1997) *J. Chem. Phys.* 67 3683-3704
 - 43 Hummer G, Garde S, Garcia A, Pohorille A, Pratt L (1996) *Proceedings of the National Academy of Science* 93:8951-8955
 - 44 Crooks G E and Chandler D (1997) *Phys Rev E* 56 4217.
 - 45 Bedard-Hearn M J, Larsen, R E, Schwartz B J (2003) *J. Phys Chem A* 107 4773-4777.